

# In situ Formation of Amorphous-Core/Crystalline-Shell Composite Powder in Liquid Immiscible Fe-Si-B-Cu System

Liu Xingjun<sup>1,2</sup>, Zhu Jiahua<sup>1</sup>, Yu Yan<sup>1</sup>, Zhang Jinbin<sup>1</sup>, Yang Shuiyuan<sup>1</sup>, Wang Cuiping<sup>1</sup>

<sup>1</sup> College of Materials and Fujian Provincial Key Laboratory of Materials Genome, Xiamen University, Xiamen 361005, China,<sup>2</sup> Department of Materials Science and Engineering, Harbin Institute of Technology, Shenzhen 518055, China

**Abstract:** Based on the CALPHAD (Calculated of Phase Diagrams) approach, micro-scale amorphous/crystalline composite powders of  $(\text{Fe}_{0.75}\text{Si}_{0.1}\text{B}_{0.15})_{100-x}\text{Cu}_x$  ( $x = 30, 45, 55, 65$ , at%) with core/shell microstructure were designed and successfully fabricated by using the gas atomization method. The obtained gas-atomized powder exhibits a Fe-Si-B-rich amorphous-core/Cu-rich crystalline-shell composite microstructure. Results indicate that the coercive force of the composite powders is almost the same as that of  $\text{Fe}_{75}\text{Si}_{10}\text{B}_{15}$  amorphous powder, but their saturation magnetization decreases with increasing Cu concentration. The formation mechanism of such amorphous-core/crystalline-shell composite powders is originated from the occurrence of liquid phase separation at high temperature and the different glass-forming ability (GFA) of the two separated liquids (Cu-rich and FeSiB-rich) during the rapid solidification process.

**Key words:** amorphous alloy; CALPHAD approach; microstructures; liquid phase separation; composites

Amorphous alloys have attracted considerable attention over the past decades due to their attractive properties such as large elastic limit, high tensile strength, excellent corrosion resistance and good soft magnetic characteristics<sup>[1]</sup>. However, in many cases, a majority of amorphous alloys fracture catastrophically under compression or tension at room temperature on account of the highly localized shear bands, which limited the applicability of amorphous alloy as engineering or structure materials<sup>[2]</sup>. Therefore, many attempts have been made to improve the plasticity of amorphous alloys. One of those is the fabrication of amorphous matrix composites, which has been proved to be an effective approach<sup>[3,4]</sup>. These composites containing a secondary ductile crystalline phase have been successfully produced by different methods in many systems, such as the *ex-situ* introduction of crystalline particles or fibers<sup>[5-7]</sup>, the nanocrystalline precipitation<sup>[8,9]</sup>, and the *in-situ* formation of crystalline

dendrites<sup>[10,11]</sup>. However, in abovementioned fabrication methods, the challenge of the inhomogeneous distribution of secondary ductile crystalline phase still exists.

Recently, liquid phase separation phenomenon has been paid widespread attention on developing *in-situ* amorphous matrix composites, including amorphous/amorphous and crystalline/amorphous composites<sup>[11-23]</sup>. In a liquid miscibility system, when the thermal melt is rapidly cooled into the liquid miscibility gap, the liquid phase separation takes place and separates into two liquids. If the two separated liquids have different glass-forming ability (GFA) in the further cooling process, then the amorphous/crystalline composite could be formed after rapid cooling process, such as melt spinning and suction casting. In addition, the gas atomization method is also a rapid solidification method, and has been widely used to produce amorphous alloys and monotectic alloys<sup>[24-27]</sup>. However, this method has not been extensively

Received date: January 12, 2019

Foundation item: National Natural Science Foundation of China (51471138, 51771158)

Corresponding author: Wang Cuiping, Ph. D., Professor, College of Materials and Fujian Provincial Key Laboratory of Materials Genome, Xiamen University, Xiamen 361005, P. R. China, Tel: 0086-592-2187888, E-mail: wangcp@xmu.edu.cn

Copyright © 2020, Northwest Institute for Nonferrous Metal Research. Published by Science Press. All rights reserved.

used in fabricating micro-scale amorphous/crystalline composites with novel microstructures. The purpose of the present work is, to design and prepare the micro-scale amorphous/crystalline composite powder in Fe-Si-B-Cu alloy system by using calculation of phase diagrams (CALPHAD) technique and gas atomization method, respectively. Then, the microstructure, thermal and magnetic properties were investigated in detail, as well as the formation mechanism of these core-shell type amorphous/crystalline composite powders.

## 1 Experiment

### 1.1 Composition design

In order to obtain the abovementioned composite powder, an immiscible alloy system should be firstly selected. We note that the Fe-Si-B-Cu system is a great candidate for this investigation. This is primarily according to the following two factors: (1) Fe-Cu system has a flat liquid line and large positive mixing enthalpy (Fig.1a), and it shows a metastable liquid miscibility below the liquids<sup>[28, 29]</sup>; (2) Fe-Si-B ternary alloy has a rather high GFA and could be prepared into fully glass ribbons up to 400  $\mu\text{m}$  in thickness, especially for  $\text{Fe}_{75}\text{Si}_{10}\text{B}_{15}$  alloy<sup>[30]</sup>.

The CALPHAD (Calculation of Phase Diagrams) technique, which has been recognized to be an important tool to reduce time and cost significantly during the development of materials, can effectively provide a clear guidance for the materials design<sup>[31]</sup>. In the present work, based on the database of Fe-based alloys which have been established by our group, a vertical section of the Fe-Si-B-Cu quaternary system for the composition cut between  $\text{Fe}_{75}\text{Si}_{10}\text{B}_{15}$  and pure Cu has been calculated, and is shown in Fig.1b. It can be seen that there exists a stable liquid-liquid phase separation region (L1+L2) with wide composition and temperature range. Fig.1c shows the calculated miscibility gap in the  $(\text{Fe}_{0.75}\text{Si}_{0.10}\text{B}_{0.15})_{100-x}\text{Cu}_x$

alloy as a function of Cu concentration. The critical temperature and the copper content of the miscibility gap is about 1657  $^{\circ}\text{C}$  and 57 at%, respectively. A stable region, a metastable region and an unstable region were divided into by binodal (solid line) and spinodal (dash line) lines. According to this vertical section, the liquid immiscible  $(\text{Fe}_{0.75}\text{Si}_{0.1}\text{B}_{0.15})_{100-x}\text{Cu}_x$  ( $x = 30, 45, 55, 65$ , at%) alloy composition was designed, and the calculated compositions of two separated liquids appear to be Fe-Si-B rich and Cu-rich, respectively.

### 1.2 Powder preparation

High purity elements of Fe, Si, Cu and a Fe-B ferroalloy ( $\geq 99.9$  wt%) with nominal composition of  $(\text{Fe}_{0.75}\text{Si}_{0.1}\text{B}_{0.15})_{100-x}\text{Cu}_x$  (at%), where  $x = 0, 30, 45, 55, 65$  (referred as Cu0, Cu30, Cu45, Cu55 and Cu65 hereafter), were firstly melted in high frequency induction furnace under an argon atmosphere. The molten alloys were heated to about 1650  $^{\circ}\text{C}$  in the crucible, which is over the liquids temperature of the selected Fe-Si-B-Cu alloys (Fig.1b), and then cast into a cylindrical cast-iron mold. After that, the master alloy ingots were remelted in a quartz nozzle surrounded by a radio-frequency induction coil. The powders with 10~150  $\mu\text{m}$  in diameter were prepared using conventional nitrogen gas atomization and the gas pressure for atomizing is about 5 MPa.

### 1.3 Analysis techniques

The surface morphologies of the powders were observed by optical microscope (OM) and scanning electron microscopy (SEM). After standard metallographic preparation, observation of cross-sectional microstructure and mapping of constituent elements in each phase of the powder were carried out by electron probe microanalyzer (EPMA) (JXA-8100R, JEOL, Japan). The crystal structure of the constituent phase was co-identified by X-ray diffraction (XRD) (X'Pert PRO-PANalytical, Philips, Netherlands) and transmission electron microscopy (TEM)

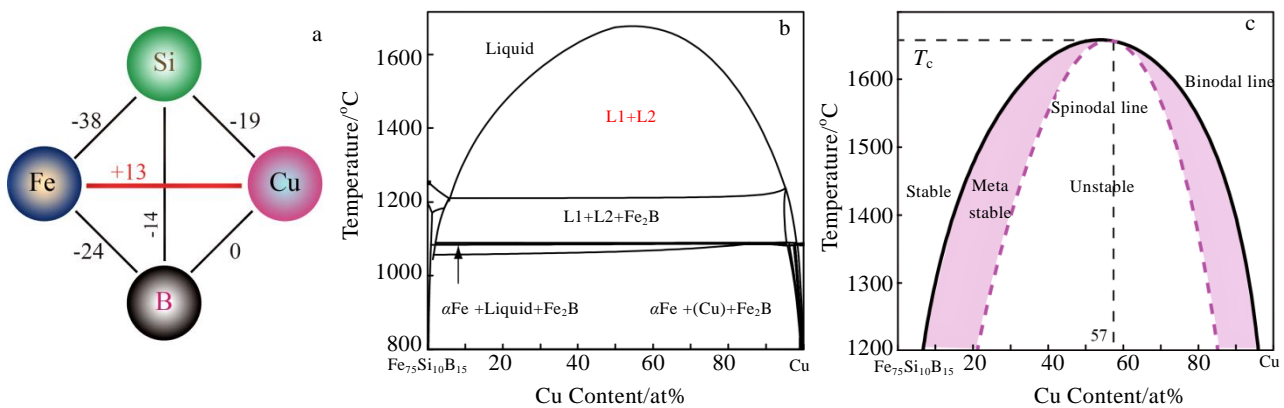


Fig.1 Relationship of heat of fusion (kJ/mol) among constituent elements in the Fe-Si-B-Cu quaternary system<sup>[24]</sup> (a); the calculated vertical section of the Fe-Si-B-Cu quaternary system for the composition cut between  $\text{Fe}_{75}\text{Si}_{10}\text{B}_{15}$  (at%) and pure Cu (b); calculated miscibility gap in  $(\text{Fe}_{0.75}\text{Si}_{0.10}\text{B}_{0.15})_{100-x}\text{Cu}_x$  alloys as a function of Cu concentration (c)

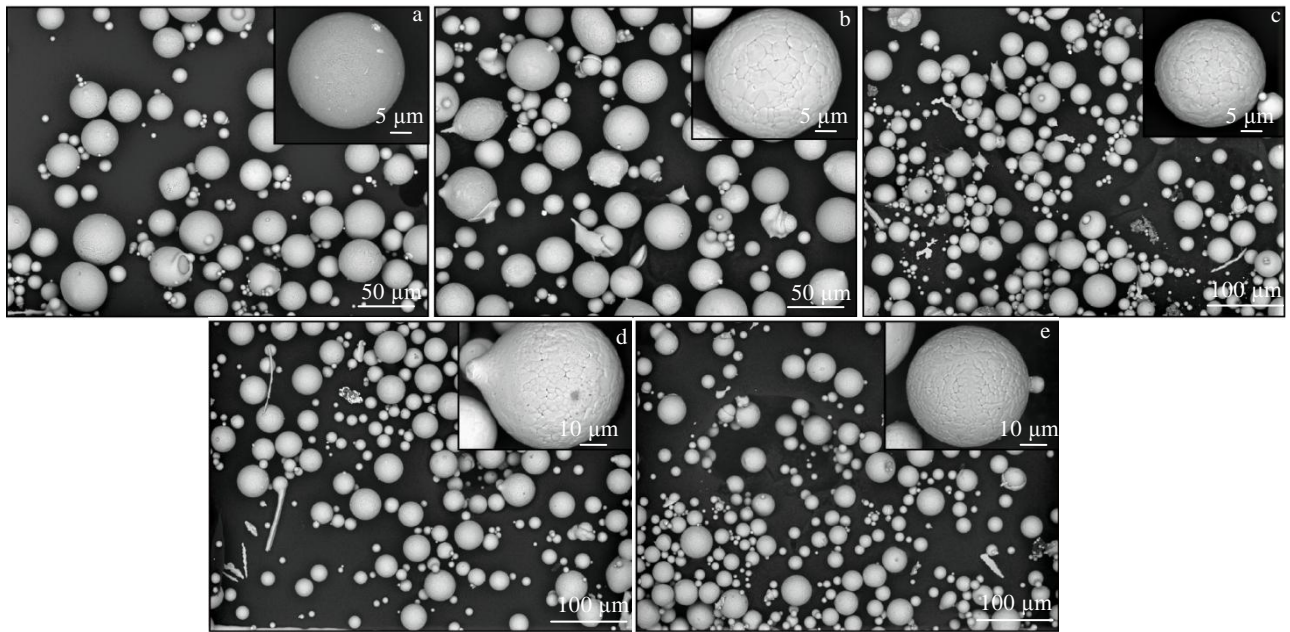


Fig.2 Surface morphologies of the gas-atomized Cu0~Cu65 powders and their corresponding magnified images (see the inset): (a) Cu0, (b) Cu30, (c) Cu45, (d) Cu55, and (e) Cu65

(JEM-2100, JEOL, Japan). The samples for TEM analysis were prepared using a focused ion beam/scanning electron microscope (FIB/SEM; FEI Helios Nano lab 600). The thermal properties of the powders were determined by differential scanning calorimetry (DSC) (DSC-404C, NETZSCH, Germany) at a heating rate of 20 °C/min using sintered Al<sub>2</sub>O<sub>3</sub> as the reference specimen. The magnetization curves of the powders at room temperature were measured using a vibrating sample magnetometer (VSM) (TVA-5, TOEIKOGYO, Japan) under a maximum applied field of  $1.28 \times 10^6$  A/m.

## 2 Results and Discussion

Fig.2a~2e show the surface morphologies of the prepared Cu0~Cu65 alloy powders, respectively. It can be seen that all the fabricated powders exhibit a good spherical morphology with clean surface. The inset images in Fig.2b~2e exhibit a large number of grain boundaries on the surface of Cu30~Cu65 powders. This indicates that the powders were fabricated well under clean atmosphere and suitable powder fabrication conditions. Fig.3 shows the cross-sectional microstructure image of the prepared powders. From the cross-section image in Fig.3a, only a single phase microstructure was observed. With the addition of Cu, the alloy powders presented a composite microstructure containing two phases (as shown in Fig.3b~3e), which is similar to our previous reports on liquid immiscible gas-atomized powders<sup>[22, 24, 26]</sup>. To analyze the composition of the two phases, a typical composite powder, i.e Cu45, was analyzed by EPMA. Fig.4 shows the

back-scattered electron (BSE) image of the Cu45 powder. In the cross-section image (Fig.4a), the gray contrast phase exhibits multi-sized circular globules dispersed in the matrix of the Cu45 alloy powders, whereas the matrix phase of the powder shows a continuous white contrast. The interface between the two phases is very smooth, which demonstrates that this core-shell microstructure was obtained through liquid phase separation phenomenon. Fig.4b~4e shows the results of mapping analysis of EPMA, indicating the distribution of constituent elements in the above composite microstructure. The inner region in gray contrast was enriched with Fe, Si, and B, while the outer region in white contrast mainly contains Cu. This can be explained by the mixing enthalpy of atomic pairs in Fe-Si-B-Cu system, as shown in Fig.1a<sup>[29]</sup>. The positive mixing enthalpy of the Fe-Cu pair and the larger negative enthalpies of Fe-Si, Fe-B and Si-B pairs imply the homogeneous liquid separated to Fe-Si-B rich and Cu-rich liquid phases. The average composition of the white and gray phases is Fe<sub>3.1</sub>Si<sub>1.8</sub>B<sub>0.3</sub>Cu<sub>94.8</sub>(at%) and Fe<sub>73</sub>Si<sub>9.5</sub>B<sub>15.2</sub>-Cu<sub>2.3</sub>(at%), respectively.

The crystal structure of constituent Fe-Si-B-rich and Cu-rich phases of the Cu0-Cu45 powder was investigated using XRD analysis, and the result is shown in Fig.5. The sharp diffraction peaks together with a broad halo peak at about  $2\theta$  from 43° to 45° (the inset in Fig.5) can be obviously seen. The sharp diffraction peaks correspond to the fcc Cu-rich crystalline phase, and the typical broad peak, similar to that for the reported Fe<sub>75</sub>Si<sub>10</sub>B<sub>15</sub>(at%) amorphous alloy<sup>[30]</sup>, implies the Fe-Si-B-rich amorphous phase

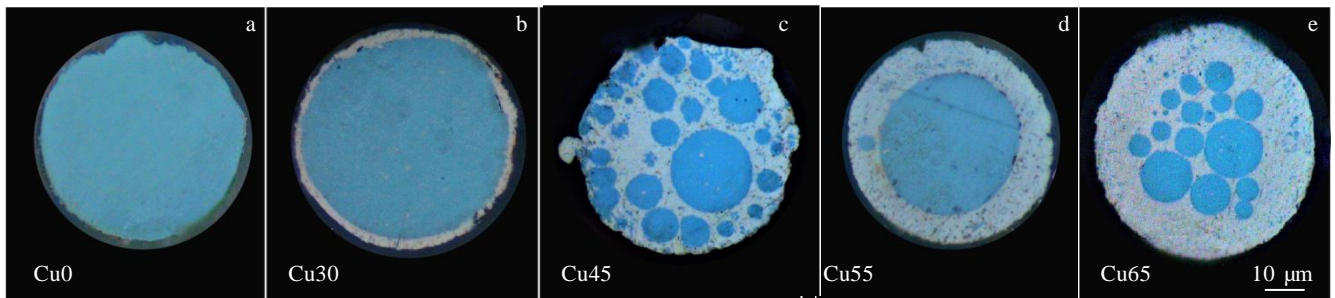


Fig.3 Cross-sectional microstructure of the gas-atomized powders: (a) Cu0, (b) Cu30, (c) Cu45, (d) Cu55, and (e) Cu65

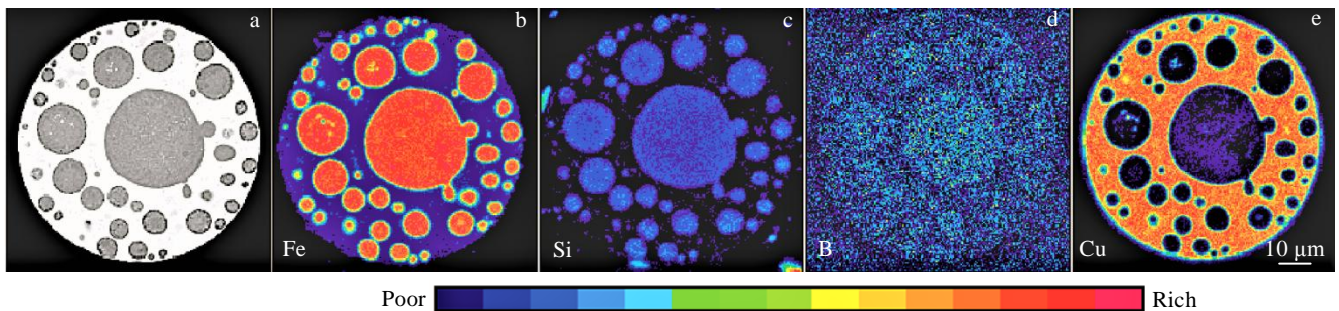


Fig.4 Cross-sectional microstructure BSE image (a) and EPMA mapping (b~e) of the Cu45 powder: (b) Fe, (c) Si, (d) B, and (e) Cu

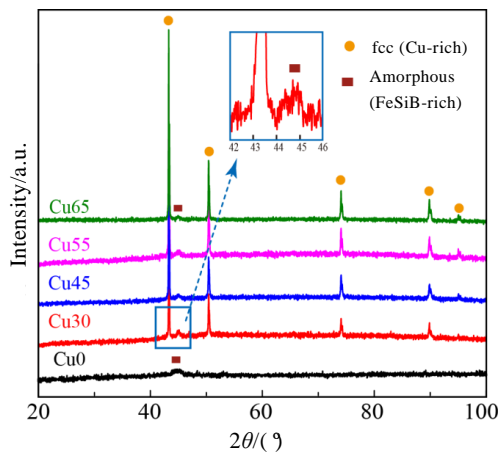


Fig.5 XRD patterns obtained from Cu0~Cu65 alloy powders

formation in the composite powders. Fig.6 shows the DSC curve of the prepared powders at a heating rate of 20 °C/min. From Fig.6a, a sharp crystallization peak can be observed. The onset crystallization temperature  $T_x$  and the first peak temperature  $T_p$  are slightly decreased with Cu addition. All the representative temperatures and thermal properties are listed in Table 1. The position and morphology of the exothermic peak is similar to that of the  $\text{Fe}_{75}\text{Si}_{10}\text{B}_{15}$  (at%) amorphous alloy<sup>[30]</sup>. In the high temperature range (900~1200 °C), as shown in Fig.6b, it is found that the powders contain Cu element presenting two endothermic peaks with onset temperatures of 1029 °C and 1089 °C. From the calculated vertical section of the

Fe-Si-B-Cu quaternary system in Fig.1b, it can be seen that there exists a three-phase region ( $\alpha\text{Fe} + (\text{Cu}) + \text{Fe}_2\text{B}$ ) at the temperature below 1050 °C. When the temperature is above 1050 °C, the (Cu) phase is changed into liquid phase (L2). With the temperature rising, the occurrence of the melting of  $\alpha\text{Fe}$  phase at about 1100 °C (L1). Thus, the first endothermic reaction can be identified as the melting of Cu-rich crystalline phase (red dotted line) with onset at  $T_m^{\text{Cu-rich}} \approx 1029$  °C. Subsequently, the last peak corresponds to the melting of the Fe-Si-B rich amorphous matrix (green dotted line) at an onset temperature  $T_m^{\text{Fe-rich}} \approx 1089$  °C.

In order to further identify the crystal structure of constituent Fe-Si-B rich and Cu-rich phases, the micro-scale Cu45 alloy powders were investigated by TEM. The bright-field (BF) micrograph of the powders clearly shows the presence of two different phases with white and dark contrast, as shown in Fig.7a. Fig.7b shows the selected area diffraction pattern (SADP) of the white contrast (marked as “A” in Fig.7a) taken along the [110] zone axis, confirming the formation of the Cu-rich crystalline phase with the *fcc* structure. Fig.7c shows the SADP of the dark contrast (marked as “B” in Fig.7a), where a halo ring is observed, indicating the formation of Fe-Si-B rich amorphous phase. Thus, it can be concluded that, the Fe-Si-B rich amorphous/Cu-rich crystalline composite powders induced by liquid phase separation has been successfully developed by using the gas atomization method.

During the gas atomization process, the thermal melt of Fe-Si-B-Cu is undercooled into the liquid miscibility gap,

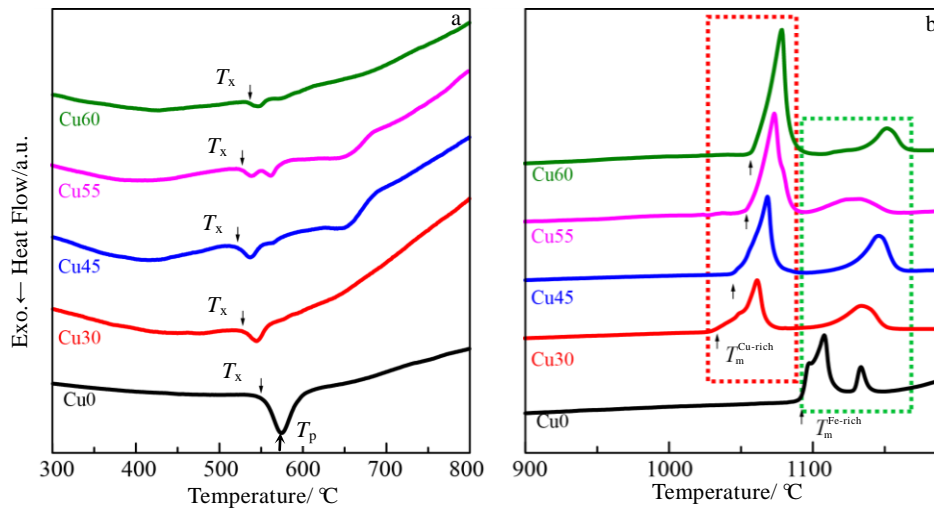


Fig.6 DSC curves obtained from Cu0~Cu65 composite powders at a heating rate of 20 °C/min by Al<sub>2</sub>O<sub>3</sub> pans: (a) the range of 300 ~800 °C; (b) the range of 900~1200 °C

**Table 1 Thermal parameters of prepared Cu0~Cu65 composite powders**

| Alloys | $T_x/^\circ\text{C}$ | $T_p/^\circ\text{C}$ | $T_m^{\text{Cu-rich}}/^\circ\text{C}$ | $T_m^{\text{Fe-rich}}/^\circ\text{C}$ |
|--------|----------------------|----------------------|---------------------------------------|---------------------------------------|
| Cu0    | 545                  | 572                  | -                                     | 1089                                  |
| Cu30   | 529                  | 543                  | 1029                                  | 1109                                  |
| Cu45   | 518                  | 535                  | 1042                                  | 1111                                  |
| Cu55   | 526                  | 538                  | 1052                                  | 1098                                  |
| Cu65   | 532                  | 555                  | 1055                                  | 1107                                  |

and the liquid-liquid phase separation will take place, which results in that the liquid separates into Cu-rich and Fe-Si-B rich liquids, followed by the aggregation of both liquids. Because of the higher GFA of Fe-Si-B rich liquid phase than that of Cu-rich liquid phase, Fe-Si-B rich amorphous/Cu-rich crystalline composite can be achieved successfully after complete solidification. The formation of the Fe-Si-B amorphous phase indicates that the Fe-Si-B liquid maintains its liquid structure at the glass transition temperature during the cooling process, resulting in the maintenance of the liquid state enough to the formation of amorphous/crystalline microstructure in the gas-atomized powders.

Fe-Si-B is a famous amorphous alloy due to its excellent soft magnetic properties, and has been widely used in transformer<sup>[1,30]</sup>. Herein, the soft magnetic properties of present (Fe<sub>0.75</sub>Si<sub>0.1</sub>B<sub>0.15</sub>)<sub>100-x</sub>Cu<sub>x</sub> ( $x = 0, 30, 45, 55, 65$ , at%) powders were investigated. Fig.8a shows the magnetization curves of the gas-atomized Cu0~Cu65 composite powders measured by VSM at room temperature with a maximum applied field of  $1.28 \times 10^6$  A/m. All of the prepared composite powders exhibit a typical characteristic of soft magnetic materials. On the one hand, these powders have low coercive force about  $8 \times 10^3$  A/m, slightly larger than Fe-Si-B amorphous powder ( $2.4 \times 10^3$  A/m). On the other hand, the saturation magnetization of above-mentioned powders significantly decreases with increasing of non-magnetic Cu content. Tian et al<sup>[32]</sup> has reported that the magnetization of Fe-Si/epoxy composites increase with increasing the content of Fe-Si magnetic powder. In the present Fe-Si-B-Cu composite powders, the Cu-rich phase is a nonmagnetic phase and has no contribution to the magnetic properties of the composite powders. Therefore, the main saturation magnetization of composite is contributed

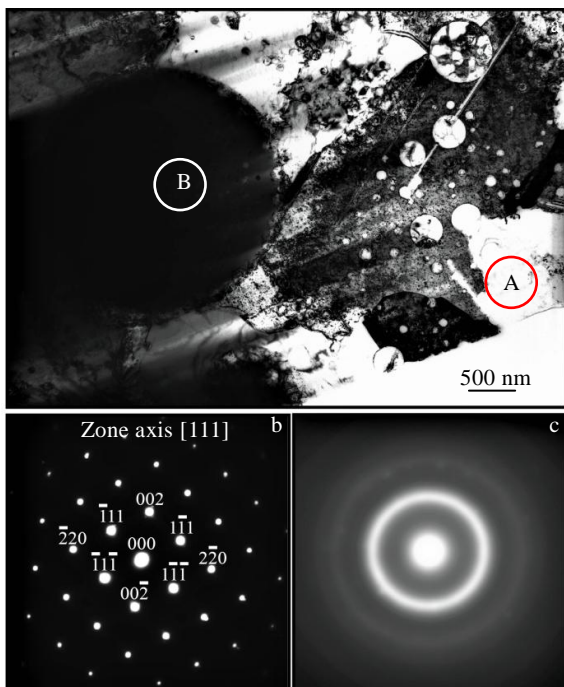


Fig.7 TEM bright field image of the gas-atomized Cu45 powder (a), SADP of region "A" in Fig.7a, showing the Cu-rich phase being a crystalline phase with the fcc structure (b), and SADP of region "B" in Fig.7a, showing the Fe-Si-B rich phase being an amorphous state (c)

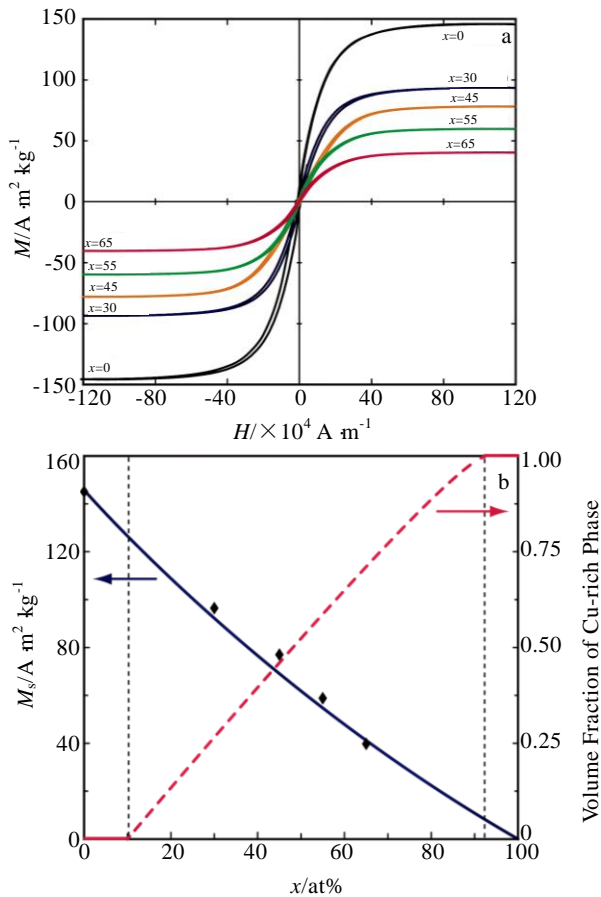


Fig.8 Magnetization curves of the gas-atomized  $(\text{Fe}_{0.75}\text{Si}_{0.1}\text{B}_{0.15})_{100-x}\text{Cu}_x$  ( $x = 0, 30, 45, 55, 65$ , at%) powders at room temperature with a maximum applied field of  $1.28 \times 10^6 \text{ A/m}$  (a); relationship of both saturation magnetization and volume fraction of Cu-rich phase ( $1300 \text{ }^\circ\text{C}$ ) via Cu concentration ( $x/\text{at}\%$ ) of above mentioned powders (b)

by volume fraction of Fe-Si-B rich amorphous phase with excellent soft magnetic properties. The relationship of saturation magnetization ( $25 \text{ }^\circ\text{C}$ ) and volume fraction of non-magnetic Cu-rich crystalline phase ( $1300 \text{ }^\circ\text{C}$ ) as a function of Cu content are presented in Fig. 8b. It can be seen that the decrease in saturation magnetization is almost linear with the increasing of Cu content. The composites prepared in this study can provide a direction for the preparation of new composite materials.

### 3 Conclusions

1) On the basis of the CALPHAD approach, the  $(\text{Fe}_{0.75}\text{Si}_{0.1}\text{B}_{0.15})_{100-x}\text{Cu}_x$  ( $x = 0, 30, 45, 55, 65$ , at%) alloys exhibiting liquid immiscibility have been pinpointed and the constituents of composite powders have been designed.

2) The composite powders consistent Fe-Si-B rich

amorphous-core/Cu-rich crystalline-shell composite microstructures were successfully produced by gas atomization.

3) The coercive force of the prepared composite powders is almost the same as that of the  $\text{Fe}_{75}\text{Si}_{10}\text{B}_{15}$  (at%) amorphous powder, but their saturation magnetization decreases with increasing Cu concentration.

4) The formation mechanism of this composite powders is the liquid phase separation of Fe-Si-B rich and Cu-rich liquids and the different GFA between these two separated liquids during the fast cooling condition.

### References

- 1 Miller M K, Liaw P. *Bulk Metallic Glasses: An Overview*[M]. Berlin: Springer Science & Business Media, 2007
- 2 Wang W H, Dong C, Shek C H. *Materials Science and Engineering: R: Reports*[J], 2004, 44(2-3): 45
- 3 Park E, Kim D. *Metals and Materials International*[J], 2005, 11(1): 19
- 4 Aversa R, Parcesepe D, Petrescu R V et al. *American Journal of Applied Sciences*[J], 2017, 14(2): 294
- 5 Conner R D, Dandliker R B, Scruggs V et al. *International Journal of Impact Engineering*[J], 2000, 24(5): 435
- 6 Qiu K Q, Wang A M, Zhang H F et al. *Intermetallics*[J], 2002, 10(11-12): 1283
- 7 Sun Y D, Chen Q R, Li G Z. *Journal of Alloys and Compounds*[J], 2014, 584: 273
- 8 Calin M, Eckert J, Schultz L. *Scripta Materialia*[J], 2003, 48(6): 653
- 9 Martin I, Ohkubo T, Ohnuma M et al. *Acta Materialia*[J], 2004, 52(15): 4427
- 10 Hofmann D C, Suh J Y, Wiest A et al. *Nature*[J], 2008, 451(7182): 1085
- 11 Wu Y, Ma D, Li Q K et al. *Acta Materialia*[J], 2017, 124: 478
- 12 Hays C C, Kim C P, Johnson W L. *Physical Review Letters*[J], 2000, 84(13): 2901
- 13 He J, Mattern N, Tan J et al. *Acta Materialia*[J], 2013, 61(6): 2102
- 14 Kim D H, Kim W T, Park E S et al. *Progress in Materials Science*[J], 2013, 58(8): 1103
- 15 Liu X, Zhu J, Yang S et al. *Materials Letters*[J], 2014, 116: 328
- 16 Mattern N, Kühn U, Gebert A et al. *Scripta Materialia*[J], 2005, 53(3): 271
- 17 Qiao J, Jia H, Liaw P K. *Materials Science and Engineering: R: Reports*[J], 2016, 100: 1
- 18 He J, Kaban I, Mattern N et al. *Scientific Reports*[J], 2016, 6: 25832
- 19 Dong Y, Wunderlich R, Biskupek J et al. *Scripta Materialia*[J], 2017, 137: 94
- 20 Wang Z Y, He J, Yang B J et al. *Materials Science and Technology*[J], 2017, 33(16): 1926
- 21 Park E S, Kim D H. *Acta Materialia*[J], 2006, 54(10): 2597
- 22 Yu Y, Takaku Y, Nagasako M et al. *Intermetallics*[J], 2012, 25: 95

- 23 Kim J, Oh H S, Kim W et al. *Acta Materialia*[J], 2017, 140: 116
- 24 Wang C P, Liu X J, Ohnuma I et al. *Science*[J], 2002, 297(5583): 990
- 25 Wang C P, Liu X J, Kainuma R et al. *Metallurgical and Materials Transactions A*[J], 2004, 35(4): 1243.
- 26 Wang C P, Liu X J, Shi R P et al. *Applied Physics Letters*[J], 2007, 91(14): 141 904
- 27 Ohnuma I, Saegusa T, Takaku Y et al. *Journal of Electronic Materials*[J], 2009, 38(1): 2
- 28 Nakagawa Y. *Acta Metallurgica*[J], 1958, 6(11): 704
- 29 Takeuchi A, Inoue A. *Materials Transactions*[J], 2005, 46(12): 2817
- 30 Inoue A, Shen B L, Chang C T. *Intermetallics*[J], 2006, 14(8-9): 936
- 31 Lukas H, Fries S G, Sundman B. *Computational Thermodynamics: the Calphad Method*[M]. Cambridge: Cambridge University Press, 2007
- 32 Tian J W, Xiao H M, Liu Y et al. *Acta Materialia Composita Sinica*[J], 2014, 21(1): 1 (in Chinese)

## Fe-Si-B-Cu 体系中原位析出非晶/晶体复合粉末的制备与性能研究

刘兴军<sup>1,2</sup>, 朱家华<sup>1</sup>, 郁炎<sup>1</sup>, 张锦彬<sup>1</sup>, 杨水源<sup>1</sup>, 王翠萍<sup>1</sup>

(1. 厦门大学, 福建省材料基因工程重点实验室, 福建 厦门 361005)

(2. 哈尔滨工业大学, 广东 深圳 518055)

**摘要:** 本研究基于相图计算的 CALPHAD 方法和超音雾化技术, 设计并制备了具有典型核/壳结构的  $(\text{Fe}_{0.75}\text{Si}_{0.1}\text{B}_{0.15})_{100-x}\text{Cu}_x$  ( $x = 0, 30, 45, 55, 65, \text{at}\%$ ) 非晶/晶体复合粉末。实验研究了该系列晶体/非晶复合粉末的显微组织, 热稳定性, 形成机理和磁性能。结果表明: 本研究制备的复合粉体均由分布在核层的富 FeSiB 非晶相和壳层的富 Cu 相组成。磁滞回线结果表明, 随着 Cu 含量的增加, 饱和磁化强度呈线性关系逐渐降低, 但对矫顽力的影响并不明显。该类非晶/晶体复合粉体的形成过程为: (1) 高温下富 Cu 相和富 FeSiB 相的液相分离现象诱发形成核/壳组织; (2) 由于富 Cu 相的玻璃形成能力远低于富 FeSiB 相, 在超音雾化过程中, 富 FeSiB 相从液态被冻结为非晶态, 最终形成具有核/壳结构的非晶/晶体复合粉体。

**关键词:** 非晶合金; CALPHAD方法; 显微组织; 液相分离; 复合材料

作者简介: 刘兴军, 男, 1962 年生, 博士, 教授, 厦门大学材料学院, 福建 厦门 361005, 电话: 0592-2187888, E-mail: lxj@xmu.edu.cn